Available online at www.sciencedirect.com
SCIENCE DIRECT
ELSEVIER
Journal of Geochemical Exploration 78–79 (2003) 279–284
JOURNAL OF GEOCHEMICAL EXPLORATION
www.elsevier.com/locate/jgeoexp

Abstract

The influence of faulting on host-rock permeability, fluid flow and ore genesis of gold deposits: a theoretical 2D numerical model

Y. Zhang[a,b,*], B.E. Hobbs[a], A. Ord[a], A. Barnicoat[c], C. Zhao[a,b], J.L. Walshe[a], Ge Lin[b]

[a] *Predictive Mineral Discovery Cooperative Research Centre, CSIRO Exploration and Mining, PO Box 1130, Bentley, WA 6102, Australia*
[b] *Guangzhou Institute of Geochemistry, Chinese Academy of Sciences, Guangzhou 510640, China*
[c] *Rock Deformation Research, School of Earth Sciences, University of Leeds, Leeds, UK*

Abstract

Veins, ore deposits and faults are often spatially related. We quantitatively explore the coupled faulting–deformation–fluid flow–chemical reaction process resulting in this association. Our 2D numerical models focus on faulting-related deformation, dilation and permeability development, fluid flow patterns, and fluid focusing/mixing locations. The models provide insight into the transport of fluids through low-permeability rocks with isolated, but more permeable faults. Mineral precipitation patterns resulting from chemical reactions during the coupled processes are also computed. The results are relevant to understanding the relationship of gold ore deposits to faults.

Keywords: Faulting; Fluid flow; Mineral precipitation; Coupled deformation–fluid flow–chemical reaction modelling

1. Introduction

It has been widely recognised that faults have enormous capability to create efficient fluid pathways in the crust, which is otherwise relatively impermeable (e.g. Knipe, 1993; Sibson, 1994). This capability is essentially determined by the mechanical role of faults in generating displacements, dilation and damage zones (e.g. Jones and Knipe, 1996; Connolly and Cosgrove, 1999). Consequently, faults are important structures controlling mineralization, as is demonstrated by the close association between faults, veins and ore deposits (e.g. Cox, 1999; Lee and Wiltschko, 2000). Advancements in our understanding of the interactions between faulting, host-rock deformation (permeability development), fluid flow and chemical reaction (mineral precipitation) are therefore critical if we are to understand the processes of mineralization.

We aim to study numerically the coupled faulting–deformation–fluid flow process through 2D numerical models. And we are particularly interested in understanding: (1) how fluids can be transported through low-permeability rocks containing isolated,

* Corresponding author. Predictive Mineral Discovery Cooperative Research Centre, CSIRO Exploration and Mining, PO Box 1130, Bentley, WA 6102, Australia. Tel.: +61-8-6436-8626; fax: +61-8-6436-8555.
E-mail address: Yanhua.Zhang@csiro.au (Y. Zhang).

0375-6742/03/$ - see front matter © 2003 Elsevier Science B.V. All rights reserved.
doi:10.1016/S0375-6742(03)00075-X

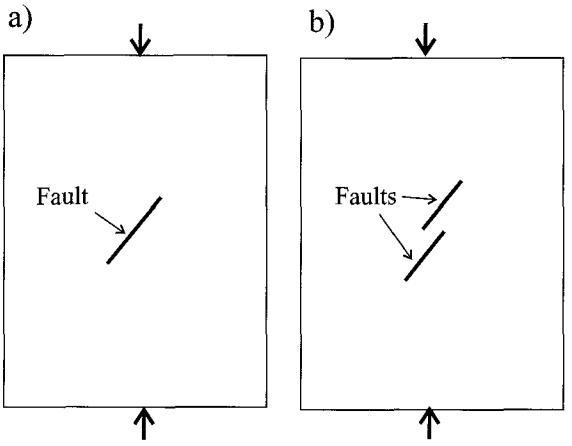

Fig. 1. Geometries of the models with one fault (a) and two faults (b). The arrows indicate the direction of the compressive loading stress. Each model lies in a horizontal plane.

but more permeable faults; (2) how high-permeability structures can develop as a result of faulting; and (3) where and why fluids are most likely to focus and mix. Simplified chemical reactions for the fluid–fluid reaction scenario during the coupled process above have also been computed. This analysis allows the prediction of mineral precipitation patterns (in this case, gold and quartz). The results are of interest in understanding the relationship of gold deposits to faults.

2. Model description

Coupled deformation–fluid flow modelling has been carried out using an explicit finite difference code (FLAC, Cundall and Board, 1988). Darcy's law for fluid flow is assumed, fully coupled with mechanical deformation. Our conceptual fault model domain simulates a 4×5-km plan (horizontal) view of a block containing isolated faults, both modelled as Mohr–Coulomb elastic–plastic, non-associative, materials (Vermeer and de Borst, 1984); gravitational forces are not considered. Such a material deforms initially in an elastic manner up to a yield point, after which it deforms in a plastic, dilatant manner. Fig. 1 shows the geometries of two models with one and two faults, respectively. A penetrative foliation (parallel to and within the faults) was incorporated into the faults; sliding along the foliation is governed by the Mohr–Coulomb failure criterion. The material properties of the models are given in Table 1. The main mechanical feature of the model is the strength contrast (cohesion and friction) between the faults/foliation and the host rock. This allows displacement along faults when the resolved shear stress along the fault/foliation reaches a critical value, generally before the host rock starts to accumulate permanent deformation. The model was loaded in compression as illustrated in Fig. 1.

To explore permeability development during the faulting process, a numerical option has been adopted to enable permeability to increase from 2×10^{-14} and 2×10^{-13} to 1×10^{-12} m^2 once the medium and fault materials fail in tension. In the model with two faults, fluid sources are applied to the top and bottom boundaries of the models to explore how these two fluids are transported though the host rock towards isolated faults. Coupling between deformation induced dilatancy and permeability increase is also included in the host-rock material. There is also a mechanical coupling between deformation induced dilatancy and fluid flow in that dilatancy produces changes in pore pressure which in turn influence fluid flow through Darcy's Law.

Table 1
Initial material properties

Model unit	Density (kg m^{-3})	Bulk modulus (Pa)	Shear modulus (Pa)	Cohesion (Pa)	Tensile strength (Pa)	Permeability (m^2)	Porosity	Friction angle (°)	Dilation angle (°)
Medium material	2500	4.7×10^{10}	2.8×10^{10}	2×10^{7}	2×10^{6}	2.0×10^{-14}	0.3	30	2
Fault	2500	4.7×10^{10}	2.8×10^{10}	2×10^{7}	2×10^{6}	2.0×10^{-13}	0.3	30	2
Foliation within faults				5×10^{6}	2×10^{6}			5	

Chemical reaction-transport modelling is carried out using a finite element code (FIDAP, Fluid Dynamics International, 1997) based on the fluid flow field resulting from the coupled deformation–fluid flow modelling. We have used a general interface (Zhao et al., 1999) to import the fluid flow field computed from FLAC into FIDAP. The chemical modelling algorithm allows mixing of a reduced hydrous fluid (CH_4-bearing) with an oxidized hydrous fluid (CO_2-bearing), and computes the related gold mineralization. The reduced fluid and the oxidized fluid are injected from the bottom and top of the computational model, respectively. Hydrogen sulphide (H_2S) is also injected from the bottom of the computational model. Both fluids are assumed to be saturated with respect to gold. Although the concentrations of the mineral-bearing fluids can vary several orders of magnitude in real geochemical systems (Barnes, 1979), the following typical values of the related concentrations are chosen in our generic model. The concentrations of the injected CH_4 and H_2S from the bottom are 0.1 and 0.01 kmol m^{-3}, respectively, whilst the concentration of the injected CO_2 from the top is 1 kmol m^{-3}. The detailed boundary conditions concerning the concentrations of the major chemical components are listed in Table 2. The mixing of these fluids as a result of the fluid flow field creates gradients in pH leading to favourable environments for gold mineralization where the fluid flow vectors cross these gradients at a high angle. The dispersion coefficient of 2×10^{-6} m^2/s is adopted in the model. Temperature is assumed to be constant throughout at 300 °C. The adoption of such temperature does not mean that our models simulate the deep levels of crust (e.g. 10 km, if assuming 30 °C /km), because the temperatures of about 300 °C have been observed at the shallow levels (about 2 km) of crust (e.g. Barnicoat et al., 1997), possibly as a consequence of hydrothermal fluid flow. Since the chemical reactions involved here are not extremely sensitive to the ambient rock pressure, this variable has not been included here.

Table 2
Boundary conditions of the related concentrations

Reactive fluids	CH_4 (kmol m^{-3})	CO_2 (kmol m^{-3})	H_2 (kmol m^{-3})	H_2S (kmol m^{-3})	Cl^- (kmol m^{-3})
Top	0.001	1.0	1×10^{-5}	0.001	0.1
Bottom	0.1	0.5	0.001	0.01	1.0

The precipitation and dissolution of gold in our chemical reaction models are controlled by the following dominant chemical reaction:

$$8Au + 16H_2S(aq) + H_2CO_3 = 8Au(HS)_2^- + 8H^+ + 3H_2O(1) + CH_4(aq)$$

3. Modelling results

3.1. Deformation and dilatant structures

The results show that the displacement distribution along a single fault is consistent with field evidence. Displacement is generally maximized at the central part of a fault and gradually decreases towards the ends of the fault. This pattern is correlated with low stresses at the central segment of the fault and high stresses at fault tips in an asymmetric pattern. There also exist two contrasting stress regimes on both sides of the fault tips, that is, a compressive domain and a tensile domain. Such asymmetry is also reflected in shear strain distributions. In the case of two adjacent faults, there is some interference in the stress fields between the two faults, but the fundamental features described above remain.

Dilatant structures develop as a result of movement along the faults. In the single fault model, this is represented by the development of a dilation zone array, analogous to wing cracks (e.g. Cox et al., 2001), at each end of the fault (Fig. 2a). In the model with two adjacent faults, simple dilation zone arrays only develop at a single end of both faults (Fig. 2b), while a major dilatant jog structure develops at the location bounded by the other ends of the two faults. These dilation patterns are analogous with some observed vein structures (e.g. Lee and Wiltschko, 2000). An analysis of failure status in the models indicates that these dilation structures are the result of tensile failure, and their locations depict approximately the locations of tensile domains, where tensile fractures are observed to develop in natural examples.

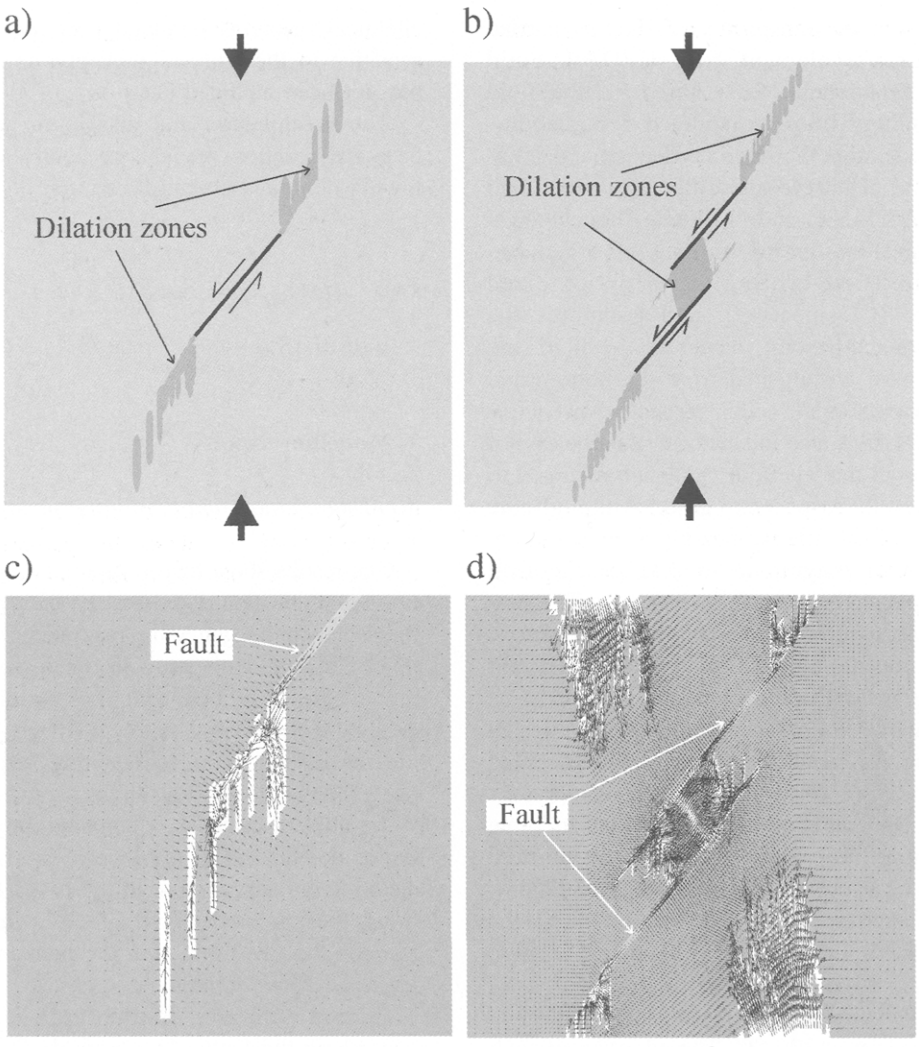

Fig. 2. (a) and (b) Dilation zones (darker grey areas) developed in the models with an isolated single fault and two isolated faults, respectively; only the central portion of the model (see Fig. 1) around the faults is plotted. The maximum volume increase in these zones is approximately 2% in (a) and 5% in (b). Arrows indicate shear sense. (c) and (d) Permeability structures and instantaneous Darcy fluid flow vectors for the model with isolated single fault (the portion of the model near the lower end of the fault) and two isolated faults (the central portion of the model), respectively. The white zones shows the locations of high-permeability structures (5×10^{-12} m^2) developed as a result of faulting. The maximum flow velocity is 1.5×10^{-6} m/s in (c) and 0.9×10^{-6} m/s in (d).

3.2. Permeability changes and fluid flow

The incorporation of permeability enhancement with tensile failure in the model enables the development of new high-permeability structures during faulting movement and deformation. These new high-permeability structures clearly coincide with dilatant structures (Fig. 2c and d). The emergence of such higher-permeability structures enhances fluid flow connectivity in the rock medium, particularly in the two-fault model where high-permeability areas became connected, forming a more efficient fluid transport network.

Fluid flow in the models (Fig. 2c and d) is strongly controlled by dilation structures and new permeability structures. While fluids are still channelled along the

pre-existing faults, the dominant fluid-flow is focused into the major dilatation zones, where fluid pore pressure generally drops, permeability is enhanced, and significant mixing occurs. Also within these dilation zones, fluid flow velocities are much greater than in other parts of the models. Note that some new higher-permeability zones where dilation is negligible only act as enhanced fluid transport conduits, rather than fluid focusing/mixing locations (Fig. 2d).

3.3. Mineral precipitation patterns

Chemical reaction-transport modelling allows us to predict the concentration gradients of relevant chemical species and the precipitation rates of various minerals. In order to ensure the accuracy of numerical computation, several attempts have been made to validate the numerical methods used for solving this kind of mineralization problem in hydrothermal systems (e.g. Zhao et al., 2000). Fig. 3 gives the precipitation patterns of gold in the one and two fault models, respectively. Note that the maximum gold precipitation rates occur in dilation zones and along some segments of the faults. Gold precipitation rates here are jointly determined by: (1) favourable structural locations (dilation zones and faults) which produce high fluid flow rates; (2) favourable geometry which promotes the possibility and efficiency of mixing of two different fluids; (3) the concentration gradients of pH. Maximum gold precipitation is only possible when all these conditions are favourable. The patchy distribution of gold precipitation arises from the rapid variations in fluid flow vectors relative to local gradients in pH. Based on the gold precipitation rates predicted by the current model, a gold deposit with a grade of about 3.5 g/t can be formed in 1.5 million years.

4. Conclusions

Our models reproduce the situation commonly observed in the field, namely, that faulting and faulting/deformation-induced permeability represent important ways to enhance the permeability of host rocks and generate fluid flow conduits for more effective mixing. This is achieved by the development of dilation zones and the generation of higher-permeability structures, both of which are simply the outcomes of tensile failure and fracturing linked to permeability increases as simulated here. This mechanism allows fluids to be transported through otherwise relatively impermeable rocks, and to focus/mix in structurally favourable locations (dilation zones or existent faults). Mineral precipitation rates depend critically on structural and fluid flow conditions and

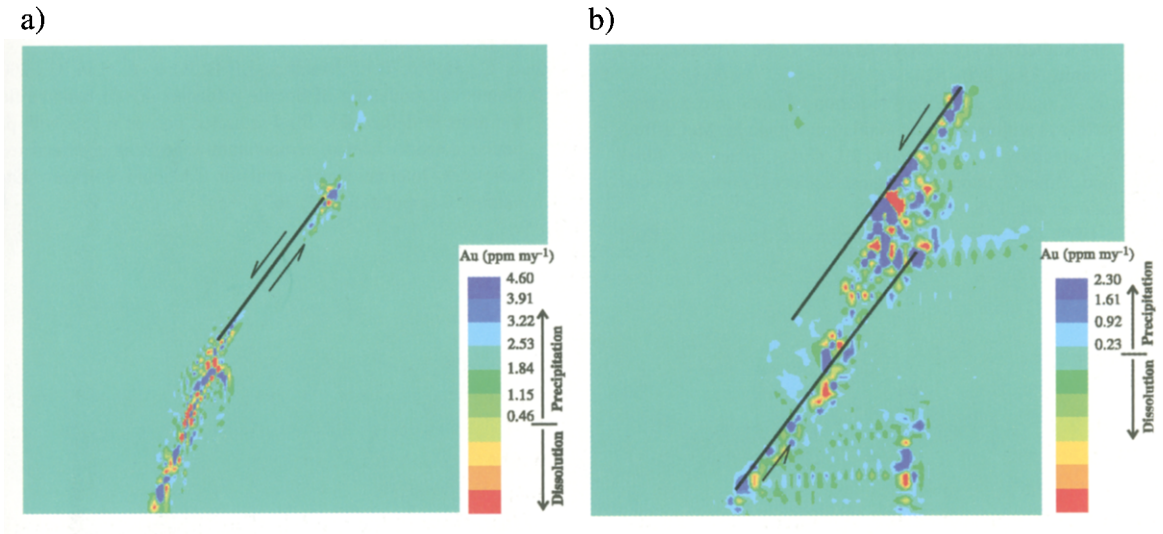

Fig. 3. (a) and (b) Distribution of precipitation rates of gold for the models with a single fault and two faults, respectively. Only the central portion of the model (see Fig. 1) is plotted. The unit of precipitation rate is ppm (by weight) per million years.

on the geometrical relation between local fluid velocity and chemical concentration gradients generated by mixing. This results in highly variable spatial mineralization sites—a situation common in nature. Maximum precipitation rates (e.g. for gold) are only possible in the dilation zones and faults where high fluid flow rates, sufficient fluid mixing and high-concentration gradients of critical chemical species are all present.

Acknowledgements

We would like to thank Grant Garven and Dr. R.A.J. Swennen for their constructive review and comments on the manuscript. Stephen Fraser and Joan Esterle are also thanked for their helpful comments on an earlier version of the paper. The authors would like thank the Chinese Academy of Sciences (Program no: KZCX2-113) and Predictive Mineral Discovery Cooperative Research Centre for financial support on the work.

References

Barnes, H.L., 1979. Geochemistry of Hydrothermal Ore Deposits. Wiley, New York.

Barnicoat, A.C., Henderson, I., Knipe, R.J., Yardley, B.W.D., Napier, R.W., Fox, N.P.C., Kenyon, A.K., Muntingh, D.J., Strydom, D., Winkler, K.S., Lawrence, S.R., Cornford, C., 1997. Hydrothermal gold mineralization in the Witwatersrand basin. Nature 386, 820–824.

Connolly, P., Cosgrove, J., 1999. Prediction of static and dynamic fluid pathways within and around dilational jogs. In: McCaffrey, K.J.W., Lonergan, L., Wilkinson, J.J. (Eds.), Fractures, Fluid Flow and Mineralization. Geological Society, London, Special Publications, vol. 155, pp. 105–121.

Cox, S.F., 1999. Deformational controls on the dynamics of fluid flow in mesothermal gold systems. In: McCaffrey, K.J.W., Lonergan, L., Wilkinson, J.J. (Eds.), Fractures, Fluid Flow and Mineralization. Geological Society, London, Special Publications, vol. 155, pp. 123–139.

Cox, S.F., Knackstedt, M.A., Braun, J., 2001. Principles of structural control on permeability and fluid flow in hydrothermal systems. Reviews in Economic Geology 14, 1–24.

Cundall, P.A., Board, M., 1988. A microcomputer program for modelling large-strain plasticity problems. In: Swoboda, C. (Ed.), Numerical Methods in Geomechanics, Proceedings of the Sixth International Conference on Numerical methods in Geomechanics, Balkema, Rotterdam, pp. 2101–2108.

Fluid Dynamics International, 1997. Fluid Dynamics Analysis Package: FIDAP. Fluid Dynamics International, IL, USA.

Jones, G., Knipe, R.J., 1996. Seismic attribute maps; application to structural interpretation and fault seal analysis in the North Sea Basin. First Break 14 (12), 449–461.

Knipe, R.J., 1993. The influence of fault zone processes and diagenesis on fluid flow. In: Horbury, A.D., Robinson, A.G. (Eds.), Diagenesis and Basin Development. Studies in Geology, vol. 36. American Association of Petroleum Geologists (AAPG), Tulsa, OK, pp. 135–154.

Lee, Y.J., Wiltschko, D.V., 2000. Fault controlled sequential vein dilation: competition between slip and precipitation rates in the Austin Chalk, Texas. Journal of Structural Geology 22, 1247–1260.

Sibson, R.H., 1994. Crustal stress, faulting and fluid flow. In: Parnell, J. (Ed.), Geofluids: Origin, Migration and Evolution of Fluids in Sedimentary Basins. Geological Society, London, Special Publications, vol. 78, pp. 69–84.

Vermeer, P.A., de Borst, R., 1984. Non-associated plasticity for soils, concrete and rock. Heron 29, 1–64.

Zhao, C., Hobbs, B.E., Mühlhaus, H.B., Ord, A., 1999. A consistent point-searching algorithm for solution interpolation in unstructured meshes consisting of 4-node bilinear quadrilateral elements. International Journal for Numerical Methods in Engineering 45, 1509–1526.

Zhao, C., Hobbs, B.E., Muhlhaus, H.B., Ord, A., Lin, G., 2000. Numerical modelling of double diffusion driven reactive flow transport in deformable fluid-saturated porous media with particular consideration of temperature-dependent chemical reaction rates. International Journal for CAE and Software: Engineering Computations 17, 367–385.